http://dx.doi.org/10.5516/NET.07.2013.093

IN-PILE PERFORMANCE OF HANA CLADDING TESTED IN HALDEN REACTOR

HYUN-GIL KIM[1*], JEONG-YONG PARK[1], YONG-HWAN JEONG[1], YANG-HYUN KOO[1], JONG-SUNG YOO[2], YONG-KYOON MOK[2], YOON-HO KIM[2], and JUNG-MIN SUH[2]
[1]Korea Atomic Energy Research Institute
989-111 Daedeok-daero, Yuseong-gu, Daejeon, 305-353, Republic of Korea
[2]KEPCO Nuclear Fuel
989-242 Daedeok-daero, Yuseong-gu, Daejeon, 305-353, Republic of Korea
[*]Corresponding author. E-mail : hgkim@kaeri.re.kr

Received October 29, 2013
Accepted for Publication January 08, 2014

An in-pile performance test of HANA claddings was conducted at up to 67 GWD/MTU in the Halden research reactor in Norway over a 6.5 year period. Four types of HANA claddings (HANA-3, HANA-4, HANA-5, and HANA-6) and a reference Zircaloy-4 cladding were used for the in-pile test. The evaluation parameters of the HANA claddings were the corrosion behavior, dimensional changes, hydrogen uptake, and tensile strength after the claddings were tested under the simulated operation conditions of a Korean commercial reactor. The oxide thickness ranged from 15 to 37 mm at a high flux region in the test rods, and all HANA claddings showed corrosion resistance superior to the Zircaloy-4 cladding. The creep-down rate of all HANA claddings was lower than that of the Zircaloy-4 cladding. In addition, the hydrogen content of the HANA claddings ranged from 54 to 96 wppm at the high heat flux region of the test rods, whereas the hydrogen content of the Zircaloy-4 cladding was 119 wppm. The tensile strength of the HANA and Zircaloy-4 claddings was similarly increased when compared to the un-irradiated claddings owing to the radiation-induced hardening.

KEYWORDS : Zr, Cladding, HANA, In-pile, Corrosion

1. INTRODUCTION

Advanced Zr-based alloys have been developed to increase the safety and efficiency of nuclear power plants for a long time because the Zircaloy currently being used has a limited service life owing to the acceleration of corrosion resistance at a high burn-up operation of a nuclear reactor. Thus, the targets of advanced Zr-based alloy development are an improvement of corrosion resistance and a decrease of the hydrogen pick-up rate during the reactor operation. To meet these needs, various Zr-based alloys, such as ZIRLO [1,2], AXIOM [2,3], M5 [4,5], E635 [6], and HANA [7,8] alloys, have been developed in many countries. Among them, ZIRLO, M5, and E635 have been used as fuel assembly components such as fuel cladding, grid spacers, or guide tubes in a present commercial reactor. The HANA alloys were developed at KAERI (Korea Atomic Energy Research Institute) for use in fuel assemblies after the systematically screen tests for the corrosion, strength, creep, and high-temperature oxidation of the various Zr-based alloy compositions. It has been reported that HANA cladding has better corrosion, creep, and high temperature oxidation performances than commercial Zircaloy-4 cladding based on the out-of-pile and in pile test [7,8].

The HANA alloy was developed at KAERI for use as a fuel assembly component such as a fuel cladding, grid spacer, or guide tube in LWRs. Previously, the in-pile tested rods of HANA cladding in the Halden research reactor in Norway were subjected to a PIE (Post Irradiation Examination), including a LOM (Light Optical Microscope), hydrogen analysis, ring tensile test, and TEM (Transmission Electron Microscopy) observation in both the matrix and oxide [8]. The irradiation conditions in the Halden test were controlled to simulate the Korean commercial reactor operations. At that time, the accumulated burn-up and fluence of the HANA claddings for PIE reached up to 34 GWD/MTU during a 3 year period. At present, the irradiation test of HANA claddings in the Halden research reactor has been conducted up to 67 GWD/MTU during a 6.5 year period of 1148 FPD (Full Power Day). The purpose of this work is to study the in-reactor performances of HANA claddings up to a high burn-up. Four types of HANA claddings (HANA-3, HANA-4, HANA-5, and HANA-6) and reference cladding (Zircaloy-4) rods were used for the irradiation test. The evaluated parameters of the HANA

test rods were the corrosion behavior, dimensional changes (creep), hydrogen uptake, and tensile strength after a burn-up of 67 GWD/MTU.

2. EXPERIMENTAL PROCEDURE

Two irradiation test rigs for HANA and reference claddings are devoted to a PWR simulation condition conducted on behalf of KAERI in the Halden research reactor in Norway. In the test rigs, typical PWR water chemistry and thermal hydraulic conditions were supplied for the test via a light water loop system [9]. During the rig test, the measured concentrations of Li and B were about 2 and 700 mg/g, respectively. The hydrogen concentration was maintained at ~ 2 mg/g, and the oxygen was not measured in the coolant by controlling the water chemistry. Regarding the coolant temperature, the measured temperature at the inlet of the test rig was ~ 280ºC with a rise in temperature through the channel of ~19ºC. The coolant flow rate was ~ 1.8 m/s, and the coolant pressure ranged from 16.6 to 16.7 MPa. The test rigs, which were composed of HANA claddings and Zircaloy-4 cladding as a reference, were installed in the Halden research reactor in February 2004, and were irradiated for a total of 13 reactor cycles (accumulated burn-up, 67 GWD/MTU) until May 2010. After six cycles of operation (November 2006) during 536 FPDs (Full Power Days), four HANA cladding rods were discharged to perform the first PIE [8].

Table 1 shows the nominal composition of HANA claddings for the in-pile test in the Halden reactor at up to 67 GWD/MTU. When compared to the HANA cladding tests between post 34 GWD/MTU [8] and 67 GWD/MTU (this work), the final annealing condition was different, as shown in table 1. Thus, a direct comparison between these two results is impossible owing to the different final annealing temperature of each HANA cladding. The axial length of the HANA test rods for the irradiation test was 350 mm. The accumulated burn-up and calculated fluence level of the HANA cladding rods reached up to 67 GWD/MTU and 2.56 x 10^{25} n/m^2 (E > 1 MeV), respectively. Owing to the physical characteristics of the Halden research reactor, the fluence level during the test was reached at ~30% when compared to the commercial reactor, although the accumulate burn-up was equal. Thus, all test results of HANA claddings were compared to the reference Zircaloy-4 cladding.

The oxide thickness, which was observed at the high heat flux region in the test rods, was measured by an ECT (Eddy Current Testing) method and LOM observation. For the LOM observation, the specimens were prepared from the sectioned samples and the observation direction was a normal plane for the cross-sectional direction of the rods to check the circumferential oxide layer. An oxide layer observation was performed on the high heat flux regions of all irradiated HANA cladding rods. The oxide thickness was measured for each captured image at four circumferential directions, and the average thickness values were calculated from the captured images. In addition, photos for the hydride distribution of cladding rods were taken from the etch-polished samples. The hydrogen content analysis was performed using ELTRA-OH-90 equipment. The specimens for the hydrogen analysis were cut from the center region of each rod, and treated in a HNO_3 solution to remove any remaining fuel particles on the inner surface, and were then ultrasonically cleaned and dried.

A ring tensile test was conducted at room temperature to obtain data on such mechanical properties as strength and ductility. Specimens for the ring tensile test, with an axial width of 2–3 mm, were cut from each tested rod around the center of the axial direction. After cutting the rods, the fuel was mechanically removed and treated in concentrated HNO_3 to remove the remaining fuel particles, and the specimens were then ultrasonically cleaned and dried. The testing was done using an Instron EZ50 tensile tester with a special jig designed at IFE for ring specimens [8]. The crosshead speed was 0.05 mm/min. The gauge length is not physically defined for the ring samples, but a nominal gauge length equal to ca. 10% of the circumference is generally considered to be appropriate. The gauge length parameters for the specimens correspond to 3.0 mm. A ring tensile test of unirradiated HANA specimens was also conducted at KAERI using the same test methods to compare the mechanical properties.

Table 1. Chemical Composition (in wt.%) and Final Annealing Conditions of HANA and Zircaloy-4 Claddings for the Halden Research Reactor Test

Cladding	Alloying element						Final annealing condition	
	Nb	Sn	Fe	Cr	Cu	Zr	34G test	67G test
HANA-3	1.5	0.4	0.1	-	0.1	Bal.	470ºC, 8h	510ºC, 8h
HANA-4	1.5	0.4	0.2	0.1	-	Bal.	470ºC, 8h	510ºC, 8h
HANA-5	0.4	0.8	0.35	0.15	0.1	Bal.	510ºC, 2.5h	470ºC, 2.5h
HANA-6	1.1	-	-	-	0.05	Bal.	470ºC, 8h	510ºC, 8h
Zircaloy-4	-	1.3	0.2	0.1	-	Bal.	SR	SR

3. RESULTS AND DISCUSSION

3.1 Corrosion and Creep Behavior of Irradiated HANA Claddings

The oxide thickness measurements of the test rods were conducted at approximately 200 day intervals using non-destructive measuring methods (ECT). Fig. 1 shows the ECT measurement result of a Zircaloy-4 test rod for the axial direction after the burn-ups of 67 GWD/MTU. The measured oxide thickness varied with the axial position of the test rod because the heat flux and coolant temperature of the test rig varied with the change in the elevated position of the test rod from the bottom to the top side. A comparison of various irradiation properties such as the oxide thickness, ring tensile result, and hydrogen content between HANA and Zircaloy-4 claddings was conducted using the high heat flux region of all test rods, as marked in Fig. 1.

Fig. 2 shows the variation in oxide thickness as a function of burn-ups up to 67 GWD/MTU [10]. The oxide thickness of all test rods increased with an increase of burn-ups, and the corrosion behavior of the test rods was followed by the parabolic rate raw. This corrosion behavior of the test rods is similar to the out-of-pile test result [11]. However, the oxide thickness of the tested rods in the Halden research reactor was about two-fold higher than that of test coupons in the PWR-simulating loop autoclave test. This increase in the oxide thickness in the in-pile corrosion test compared to the out-of-pile corrosion test was caused by the irradiation damage and heat flux effect on the test cladding [12]. In addition, the transition behavior of the oxidation rate was clearly shown in the HANA test rods at a burn-up of 40 GWD/MTU. However the transition behavior of the oxidation rate was unclear in the Zircaloy-4 cladding. It is thought that the corrosion transition of Zircaloy-4 cladding occurred at a lower burn-up than the HANA claddings, and therefore the measuring intervals used in this experimental procedure cannot be covered for the observation of the transition behavior of Zircaloy-4.

Although the oxide thickness measurement by ECT was successfully used to measure the oxide thickness without

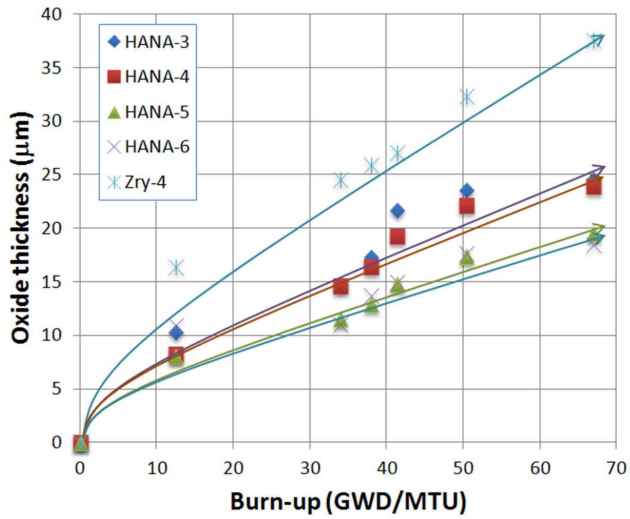

Fig. 2. Corrosion Behavior of HANA and Zircaloy-4 claddings Tested at the Halden Research Reactor Up to Burn-ups of 67 GWD/MTU [10]

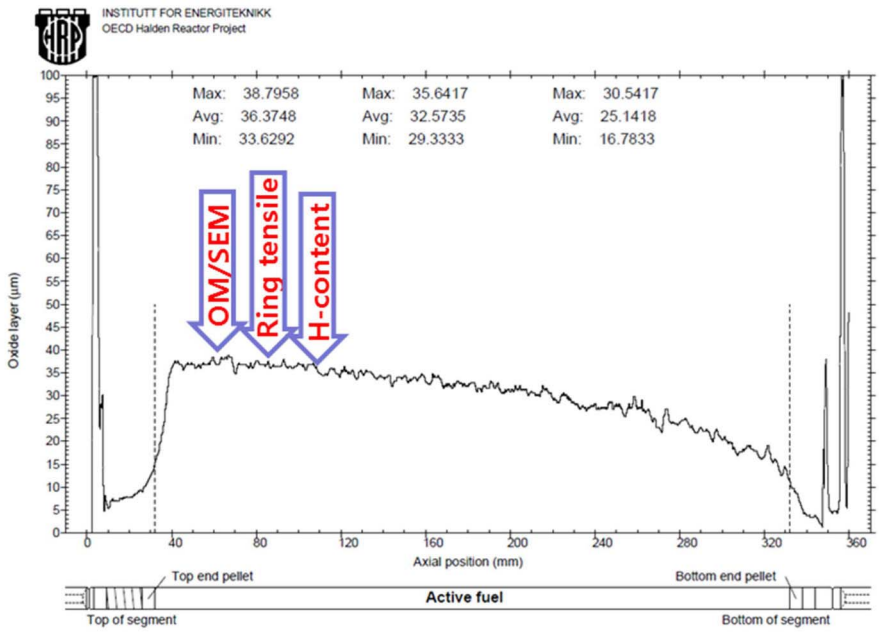

Fig. 1. Oxide Thickness Measurement Results to the Axial Direction of Zircaloy-4 Test Rod Tested at the Halden Research Reactor after Burn-ups of 67 GWD/MTU

damaging the fuel rods, the measured value of the oxide thickness has to be confirmed through a destructive test because of the inherent measuring error of the ECT technique. Thus, the LOM observation was applied in this work for the test rods of up to 67 GWD/MTU. The purpose of the LOM examination was to determine the oxide thickness and presence of defects at the metal/oxide interface and oxide layer. From the LOM observation of the oxide layer, as shown in Fig. 3, the oxide thicknesses of all HANA claddings were thinner than the Zircaloy-4 cladding, and the oxide thickness measurement results by LOM were somewhat lower when compared to the results obtained by the ECT technique as shown in Fig 4. This difference of oxide thickness between the LOM and ECT measurements is related to the inaccurate factor of the ECT measurement caused by calibration errors. Thus, an evaluation of the oxide thickness after an irradiation test is acceptable when the LOM measurement result is used. In addition, lateral cracks in the oxide layer can be identified in some cladding rods such as HANA-4, HANA-5, and Zircaloy-4. The frequency of the lateral cracks was greater in the Zircaloy-4 oxide layer than in the HANA-4 and HANA-5 oxide layers. However, the lateral cracks were not observed in the HANA-3 and HANA-6 oxide layer. Regarding the lateral crack formation in the oxide layer, the lateral cracks can be formed when a locally non-protective area was formed in the oxide layer [13]. Thus, the protectiveness of the oxide layer formed on HANA-3 and HANA-6 claddings is superior to that of the oxide layer formed on HANA-4, HANA-5, and Zircaloy-4 claddings during the irradiation test. Work to elucidate the reasons for the improved corrosion resistance of the HANA alloys over Zircaloy-4 has been recently reported [8, 10], with particular reference to the HANA-4 and HANA-6 alloys. From the observation of the oxide microstructure of the HANA alloys tested in the Haden reactor, it was revealed that the oxide consisted mainly of columnar grains in the interface region as well as in the intermediate region of the oxide layer. The precipitates incorporated in the oxide maintained crystalline from at the interface region, but transformed into an amorphous state when far away from the interface to the outer region. The precipitates in the HANA alloys were more finely distributed and oxidized more slowly in the oxide compared with Zircaloy-4. Such oxidation characteristics of the precipitates, along with the reduction in Sn content and the addition of Nb content, were considered to be more favorable for growing oxide without crack formation in the oxide layer. As summarized based on the in-pile corrosion behaviors, it is known that the oxide thickness, which was measured at the high heat flux region in test rods using the LOM method, ranged from 12 to 36 μm after the 1148 FPD. All HANA claddings showed better corrosion behavior than Zircaloy-4 cladding in the in-pile test condition.

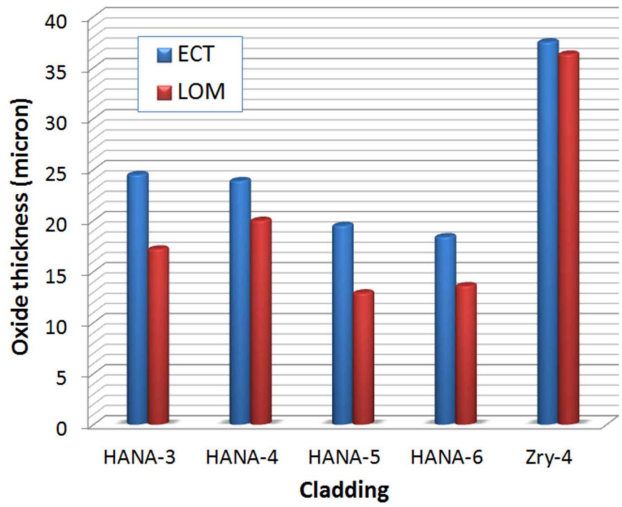

Fig. 4. Comparison of Oxide Thickness between ECT and LOM Measurement of HANA and Zircaloy-4 Claddings Tested at the Halden Research Reactor after Burn-ups of 67 GWD/MTU

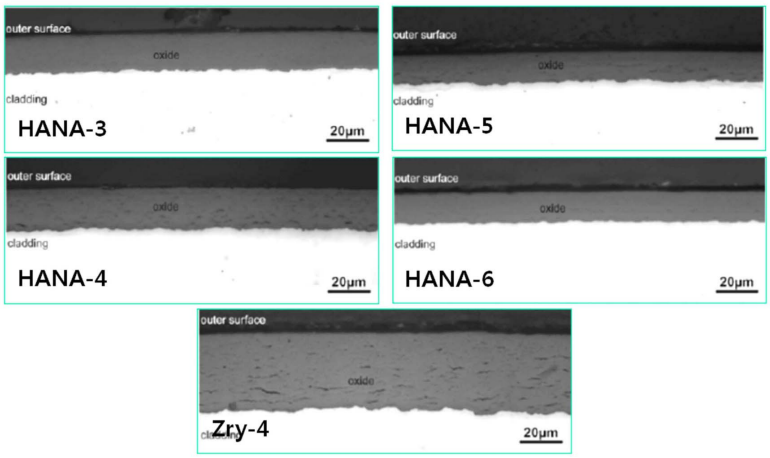

Fig. 3. Cross-section LOM Observation of Oxide Layer of HANA and Zircaloy-4 Claddings Tested at the Halden Research Reactor after Burn-ups of 67 GWD/MTU

Fig. 5 shows the tube diameter measurement results as a function of irradiation burn-ups, which were corrected for the oxide thickness to evaluate the free cladding diameter variation without the oxide thickness effect. Initially, the rod diameter decreased to be up to about 34 GWD/MTU; however, the measured diameter increased with an increase in the test burn-up, which was affected by the fuel swelling behavior after the fuel-clad interaction. This inverse trace in diameter change was related to the pellet-clad mechanical interaction (PCMI), which was identified by a ridged pattern in the axial diameter measurement results. In addition, the ridges can be seen for all test rods after the burn-ups of 34 GWD/MTU. To compare the free creep behavior of the HANA and Zircaloy-4 claddings, it is necessary to use data from the period before fuel-clad interaction occurred. Because evidence of fuel-clad interaction in the majority of the fuel rods was obtained after 12 GWD/MTU, marked as the dotted line in Fig. 5, the free creep behavior of HANA and Zircaloy-4 claddings can only be evaluated from the test results after burn-ups of 12 GWD/MTU. As shown in Fig. 5, all of the HANA claddings showed superior creep resistance to that of the Zircaloy-4 cladding. In particular, the creep down of HANA-4 was less than half of that of the Zircaloy-4 cladding.

The difference in the creep deformation in the HANA claddings was caused by the optimized combination between the alloying elements and the recrystallization fractions. It is well known that the creep resistance of zirconium-based alloys is determined by the recrystallization fractions [14, 15]. Since the four types of HANA claddings have a partial recrystallized grain, the creep deformation was decreased when compared to the Zircaloy-4 cladding, which has a stress relief structure. Regarding the alloy composition, it is well known that the creep strength of zirconium alloys is affected by alloying elements such as tin, niobium, oxygen, carbon, and sulfur in a solid solution [16]. In the HANA alloys, the alloying compositions were effectively controlled for enhancing the creep strength at concentrations in the soluble limits. However, the lower creep resistance of HANA-6 cladding than other HANA claddings was caused by the absence of Sn in HANA-6 alloy.

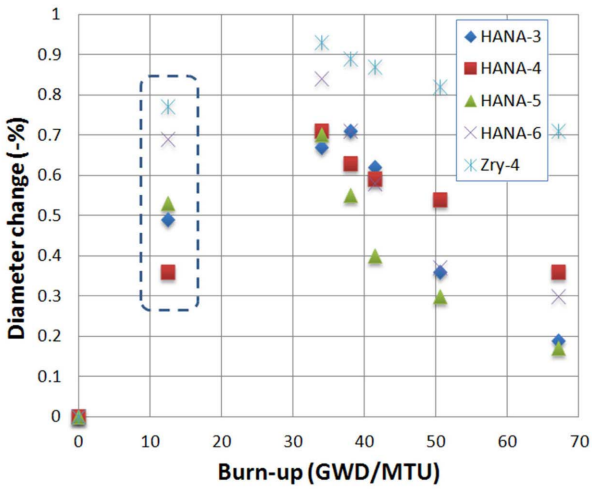

Fig. 5. Tube Diameter Variation Behavior of HANA and Zircaloy-4 Claddings Tested at the Halden Research Reactor up to Burn-ups of 67 GWD/MTU [10]

3.2 Hydride Properties of Irradiated HANA Claddings

Hydrogen generation occurred by the corrosion reaction between coolant water and zirconium alloy on the surface of zirconium alloys in a reactor operation environment. The generated hydrogen can be diffused into the zirconium alloy matrix through the ZrO_2 layer, which was precipitated to the hydride in the zirconium matrix when the hydrogen content was higher than the solubility in the zirconium matrix [17]. Regarding the hydride formation in the zirconium alloy, the cladding integrity is affected by the hydride formation because the cladding failure was considerably affected by the radial hydride on the cladding and hydride rim/blister formation [18, 19]. Thus, hydrogen pick-up behavior is undesirable in the zirconium cladding, and the hydride direction and distribution can be controlled to improve the cladding integrity.

Fig. 6 shows the hydride morphologies of the HANA and Zircaloy-4 claddings after burn-ups of 67GWD/MTU. The observed hydrides in both HANA and Zircaloy-4 claddings were randomly distributed in the matrix and their orientation was well developed in the circumferential

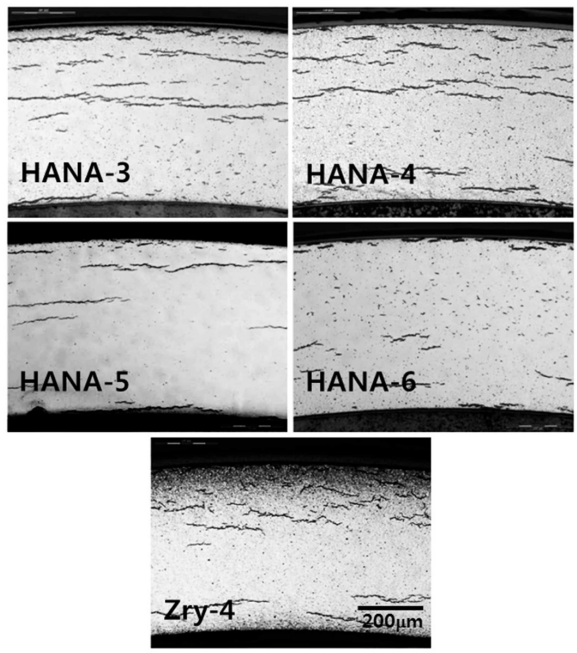

Fig. 6. LOM Observation of the Hydride Morphologies of HANA and Zircaloy-4 Claddings Tested at the Halden Research Reactor after Burn-ups of 67 GWD/MTU

direction on the tubes. The frequency of observed hydride was increased on the outer side of the cladding tubes, because the hydride precipitation was preferable to the low temperature region. The fraction of observed hydride was much lower in HANA-6 than in other cladding materials. Because all of the hydrides in the HANA claddings ware oriented toward the circumferential direction in the cladding tube shape, it is expected that the expected cladding failure owing to the radial hydride orientation can be suppressed. It was also found that hydride rims/blisters were not observed in the HANA cladding tubes at the high heat flux region after the burn-ups of 67 GWD/MTU.

Table 2 shows the analyzed hydrogen content of the HANA and Zircaloy-4 claddings. A correlation between hydride morphology and analyzed hydrogen content did not directly appear in irradiated cladding materials, because the LOM observation of hydride morphology can be affected by the sample preparation techniques such as grinding, etching, and drying. However, the hydrogen content analysis was reliable because the analyzed results were averaged from the three sample tests for each cladding. The hydrogen contents of the HANA claddings ranged from 54 to 96 wppm at the high heat flux region of the test rods. These results are lower than the Zircaloy-4 cladding of 119 wppm.

Table 2. Analyzed Hydrogen Contents of HANA and Zircaloy-4 Claddings Tested in the Halden Research Reactor for Burn-ups of 67 GWD/MTU

Cladding	Analyzed hydrogen content (wppm)
HANA-3	96
HANA-4	67
HANA-5	65
HANA-6	54
Zircaloy-4	119

It can be seen that the analyzed hydrogen content of HANA claddings is lower than that of Zircaloy-4 cladding. Among the analyzed hydrogen contents of HANA claddings after the Halden research reactor test, the HANA-6 cladding showed the lowest value, and the HANA-3 cladding showed the highest value. A correlation between the oxide thickness and analyzed hydrogen content was well matched in the four types of HANA cladding materials.

3.3 Ring Tensile Properties of Irradiated HANA Claddings

Ring tensile test results of the YS (Yield Strength), UTS (Ultimate Tensile Strength), and TE (Total Elongation) values on the HANA and Zircaloy-4 claddings are shown in table 3. In the ring tensile test of the irradiated cladding tubes, the oxide thickness of the ring shape specimens was not considered because the peeling of the oxide layer from the irradiated cladding tubes was very difficult. The effect of oxide thickness was corrected in the sample area of the ring tensile specimens. The YS and UTS of the irradiated samples were considerably increased when compared to the values of un-irradiated samples of HANA and Zircaloy-4 claddings, whereas the TE was decreased after the irradiation. The tensile strength of the HANA and Zircaloy-4 claddings was similarly increased when compared to the un-irradiated claddings.

The variations of ring tensile property results changed with the alloy compositions and the final annealing conditions of the tested cladding materials. Low temperature annealed claddings such as HANA-5 and Zircaloy-4 showed a lower strength increment than other claddings such as HANA-3, 4, and 6, as shown in table 1. In the previous results of the ring tensile test for the irradiated HANA claddings during the 1.33×10^{25} n/m^2 (E > 1 MeV) fluence [8], the HANA-5 cladding showed a higher variation of strength and ductility than the other claddings after the irradiation test. Because the HANA-5 cladding was annealed at higher temperature than the other HANA claddings, as shown in

Table 3. Ring Tensile Test Results of HANA and Zircaloy-4 Cladding Rods before Irradiation and after Irradiation of 2.56×10^{25} n/m^2 (E > 1 MeV) Fluence during the Halden Research Reactor Test

Cladding	Ring tensile test					
	Before irradiation			After irradiation		
	YS, MPa	UTS, MPa	TE, %	YS, MPa (%*)	UTS, MPa (%*)	TE, % (%*)
HANA-3	595	706	23.6	690 (15.9)	813 (15.2)	10.1 (-57.2)
HANA-4	582	697	22.9	674 (15.8)	798 (14.5)	9.7 (-57.6)
HANA-5	659	800	19.7	688 (4.4)	825 (3.1)	7.4 (-62.4)
HANA-6	412	517	24.2	591 (43.4)	685 (32.5)	8.5 (-64.9)
Zircaloy-4	595	715	22.0	638 (7.2)	764 (6.9)	7.6 (-65.5)

*: *variation percent (%) of each result compared to the before irradiation test result*

table 1, the fraction of recrystallized grains was higher. It can be summarized that the increased strength of the HANA claddings by irradiation was caused by a saturation of a-type dislocations in the recrystallized matrix from the microstructural analysis using TEM [8]. Of course, the accumulated burn-up and initial microstructure of the HANA claddings between this work and the previous work [8] were somewhat different. However, it is expected that the radiation-induced hardening of HANA cladding is similar in both cases. In addition, the deformation bands, as well as the shear fracture mode, can be seen in both cases at the surface at the deformed region of the ring tensile test. From this, the HANA-6 cladding, which has the largest recrystallization fraction in a matrix of the tested claddings, showed a higher variation of strength and ductility than the other claddings after the irradiation test.

Fig. 7 shows the fractured shapes after the ring tensile test and SEM observation of the fractured surface of irradiated HANA and Zircaloy-4 cladding rods tested in the Halden research reactor. The oxide layer fracture and deformation bands can be seen on the surface at the deformed region of the ring shape samples. The direction of the deformation bands ranged from 35 to 45° in the tensile direction, and the fractured direction of the tested specimens matched the direction of the deformation band. From the SEM observation of the fractured surface after the ring tensile test for the irradiated cladding materials, many dimples were observed in the fractured surface. The formation of the dimples of the irradiated zirconium alloy is related to the plastic deformation, which occurred by gliding dislocations and channeling these dislocations inside narrow bands of the grain [20]. Based on a comparison of the fractured surface for the ring tensile tested samples, the dimple size of HANA-5 and Zircaloy-4 was considerably decreased when compared to the size of the HANA-3, 4, and 6 claddings. Thus, it is known that the variation in strength and dimple size was well matched in the irradiated cladding materials. In the fractured surface images, the interesting point is that crack opening is frequently observed in the fractured surfaces. This crack formation is caused by the hydride formed in the matrix during the irradiation corrosion test, because the direction and size of this crack pattern is well matched with the hydride images as shown in Fig. 6. It was recognized that the irradiation ductility of HANA-3, 4, and 6 claddings is better than that of HANA-5 and Zircaloy-4 claddings from the TE and fractured surfaced observation results.

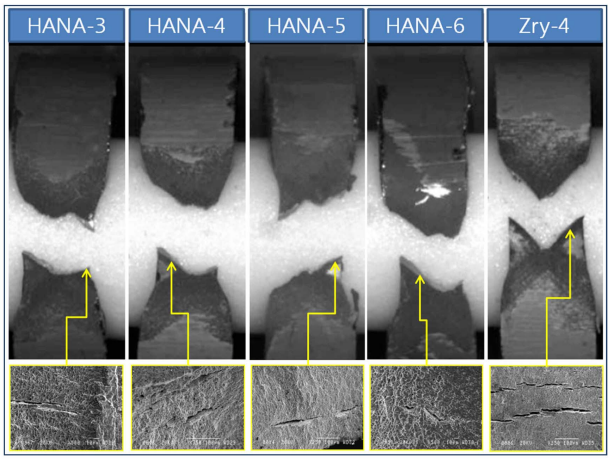

Fig. 7. Fractured Shape after Ring Tensile Test and SEM Observation of a Fractured Surface of the Irradiated HANA and Zircaloy-4 Cladding Rods Tested in the Halden Research Reactor

4. CONCLUSIONS

An irradiation test of HANA cladding was successfully conducted at the Halden research reactor at IFE in Norway. The accumulated burn-up and calculated fluence levels of the HANA and Zircaloy-4 claddings reached up to 67 GWD/MTU and 2.56 x 10^{25} n/m^2 (E > 1 MeV), respectively. The conducted evaluation items were the oxide thickness and diameter measurement with the test burn-ups, LOM observation of the oxide layer, hydrogen content analysis, and ring tensile test. All HANA claddings showed an improved corrosion resistance compared to the Zircaloy-4 cladding, and all HANA claddings showed a lower creep-down behavior than the Zircaloy-4 cladding. The hydrogen content of the HANA claddings was analyzed to be in the range of 54 to 96 wppm. These results are lower than the hydrogen content of Zircaloy-4, which is 119 wppm at a high heat flux region of the test rods. The ring tensile strengths of the HANA-3 to 6 and Zircaloy-4 claddings were similarly increased when compared to the un-irradiated claddings after the burn-up of 67GWD/MTU in the Halden research reactor test.

ACKNOWLEDGEMENTS

This work was supported by the National Research Foundation of Korea (NRF) grant funded by the Korean government (MSIP) (No. 2013M2A8A5000702). The authors would like to thank IFE in Norway.

REFERENCES

[1] R.J. Comstock, G. Schoenberger, G.P. Sabol, ASTM STP 1295 (1996) 710–725.
[2] A.M. Garde, R.J. Comstok, G. Pan, R. Baranwal, L. Hallstadius, T. Cook, F. Carrera, J. ASTM Int. 7 (2010). Paper ID JAI103030.
[3] G. Pan, C.J. Long, A.M. Garde, A.R. Atood, J.P. Foster, R.J. Comstock, L. Hallstadius, D.L. Nuhfer, R. Baranwal, in: Proceedings of 2010 LWR FuelPerformance/TopFuel/ WRFPM, Orlande, Florida, USA, September 26–29, 2010, Paper 0074.
[4] J.P. Mardon, D. Charquet, J. Senevat, ASTM STP 1354 (2000) 505–524.
[5] V. Chabretou, P.B. Hoffmann, S. Trapp-Pritsching, G. Garner,

P. Barberis, V. Rebeyrolle, J.J. Vermoyal, J. ASTM Int. 8 (2010). Paper ID JAI103013.
[6] A.V. Nikulina, Y.K. Bibilashvili, P.P. Markelov, M.M. Peregu, V.A. Koterekhov, A.F. Lositsky, N.Y. Kuzmenko, Y.P. Shevnin, V.K. Shamardin, G.P. Kobylyansky, A.E. Novoselov, ASTM STP 1295 (1996) 785–804.
[7] K.W. Song, Y.H. Jeong, K.S. Kim, J.G. Bang, T.H. Chun, H.K. Kim, K.N. Song, Nucl. Eng. Technol. 40 (1) (2008) 21–35.
[8] H.G. Kim, B.K. Choi, S.Y. Park, Y.I. Jung, D.J. Park, J.Y. Park, J. Nucl. Mater, 426 (2012) 173-181.
[9] P.J. Bennett, in: Summary of the results from the third interim inspection of fuel rods from the KAERI PWR corrosion tests IFA-673, IFA-674 and OFA-697, HR-41, February 2007.
[10] H.G. Kim, J.Y. Park, Y.I. Jung, D.J. Park, Y.H. Koo, TopFuel 2012, Manchester, United Kingdom, 2 - 6 September 2012.
[11] J.Y. Park, B.K. Choi, S.J. Yoo, Y.H. Jeong, ASTM Int. 5 (5) (2008). Paper ID: JAI101129.
[12] F. Garzarolli, H. Stehle, and E. Steinberg, Zirconium in the Nuclear Industry, ASTM STP 1295 (1996) 12-32.
[13] H.G. Kim, J.Y. Park, Y.H. Jeong, J. Nucl. Mater, 345 (2005) 1-10.
[14] R.J. Beauregard, G.S. Clevinger, K.L. Murty, Effect of annealing temperature on the mechanical properties of Zircaloy-4 cladding. In: Proceedings of the 4th International Conference SMiRT. San Francisco, CA, C3/5 (1977).
[15] K. Källström, T. Andersson, A. Hofvenstam, Zirconium in the Nuclear Industry. ASTM STP 551, (1974) 160-168.
[16] H.G. Kim, Y.H. Kim, B.K. Choi, Y.H. Jeong, J. Nucl. Mater, 359 (2006) 268-273.
[17] P. Morize, J. Baicry, J.P. Mardon, ASTM STP 939 (1987) 101–119.
[18] M. Nakatsuka, S.K. Yagnik, in: 16th International Symposium: Zirconium in the Nuclear Industry, ASTM, Chendu, China, May 2010.
[19] M. Nakatsuka, K. Sakamoto, and T. Higuchi, in: Proceedings of the 2010 LWR Fuel Performance/TopFuel/ WRFPM, Orlando, Florida, USA, September 26–29, 2010, Paper 015.
[20] F. Onimus, I. Monnet, J.L. Béchade, C. Prioul, P. Pilvin, J. Nucl. Mater. 328 (2004) 165–179.